Journal of Applied Electrochemistry **33**: 311–317, 2003.

Aspects of electrochemical behaviour of carbon steel in different Bayer plant solutions

L. GAVRIL[1], R. BREAULT[1,2] and E. GHALI[1,*]
[1]*Université Laval, Ste-Foy, Québec, Canada G1K 7P4*
[2]*Alcan International Limited, 1955 boul. Mellon, Jonquière, Québec, Canada G7S 4K8*
*(*author for correspondence)*

Received 16 July 2001; accepted in revised form 10 December 2002

Key words: alumina, Bayer solution, carbon steel, oxide films

Abstract

Cyclic voltammetric and potentiodynamic studies were carried out on 300W carbon steel in Bayer plant solution, at 100 °C, with different alumina concentrations. Alumina behaves as an anodic inhibitor, shifting the critical passivation potentials positively and decreasing the critical passivation current with increasing concentration. Increase in alumina concentration promotes the formation of a uniform and less porous film. The pore resistance model describes the properties of the oxide films. Aluminium was found in all oxides formed, supporting the formation of a mixed oxide $Fe_{3-x}Al_xO_4$. Thermodynamic calculation of some equilibrium potentials was carried out using the $Fe(OH)_3^-$ ion rather than $HFeO_2^-$ ion. Moreover, the $Al(OH)_4^-$ ion was considered instead of AlO_2^- ion in the oxidation process.

1. Introduction

In the Bayer process hot caustic solutions are used to dissolve bauxite, a mineral containing alumina. The presence of aluminate ion in these solutions has a direct impact on the carbon steel, the material commonly used for the tanks. In spite of its importance in the production of alumina, the influence of alumina concentration on the oxide film formed in Bayer pregnant liquor or at intermediate concentrations was not systematically studied. Limited investigation has been carried out on the influence of aluminate ions (AlO_2^-) on the electrochemical behaviour of carbon steel in caustic solutions. Sriram and Tromans [1] studied the influence of aluminate ions on anodic polarization of carbon steel in hot NaOH solutions. They found that the presence of aluminate ions inhibits anodic dissolution and reduces peak current density in the active–passive transition. This behaviour was explained by the adsorption of aluminate anions on the surface and to the formation of a mixed amorphous film ($Fe_{3-x}Al_xO_4$, $x \leqslant 2$). Liu et al. [2], in their study on mild steel in caustic aluminate solutions at 260 °C, found that the presence of AlO_2^- reduces the potential range for stress corrosion cracking (SCC). They also found that aluminate ions make the film more stable and protective, leading to less crack propagation during SCC process. The films formed were reported to be made of $Fe_{3-x}Al_xO_4$ ($x \leqslant 2$) and $(Fe, Mn)_{3-x}Al_xO_4$ ($x \leqslant 2$). However, these films were not amorphous as those described in [1]. Le and Ghali [3] studied the susceptibility of carbon steel to SCC in the presence and absence of AlO_2^- in hot caustic and Bayer solutions. They concluded that the presence of aluminate ions makes carbon steel more susceptible to SCC because of the formation of an amorphous film, as reported in [1].

In the present study, aspects of electrochemical behaviour of carbon steel were investigated in Bayer plant liquor with different aluminate ion concentrations.

2. Experimental details

2.1. *Material*

Plates of 300W carbon steel (CAN/CSA–G40.21-M92), with chemical composition mentioned in Table 1, were machined to obtain cylindrical electrodes of ~7 mm in diameter and ~6 mm in height, that is, same thickness as the plate. Before each experiment, these electrodes were mechanically polished with emery paper up to 600 grit, rinsed with distilled water, alcohol and acetone and dried.

2.2. *Electrolytes*

The general behaviour of 300W carbon steel in caustic solution was evaluated in pure 2.25 M NaOH solution at 30 °C and 100 °C, using cyclic voltammetry method. Bayer plant liquors with different concentrations of dissolved alumina (g l^{-1} as Al_2O_3) were used: 75, 105, 130 and 150 g l^{-1}. The Bayer liquor containing 75 g l^{-1}

Table 1. Chemical composition of 300W steel (wt %)

C	Mn	Al	S	Si	Cu	Ni	Cr	Mo	Fe
0.208	0.868	0.036	0.011	0.046	0.109	0.019	0.031	0.008	98.63

of dissolved alumina is usually named spent liquor, whereas the most concentrated solution, at 150 g l^{-1}, is called the pregnant liquor. These liquors were sampled at Alcan's Vaudreuil Plant and they contained mainly ~4.3 M NaOH and ~0.35 M Na_2CO_3. Liquors containing 105 and 130 g l^{-1} of alumina were obtained by mixing, in different proportions, spent and pregnant liquors (2:1 and 1:2, respectively). All the solutions were used at 100 ± 1 °C and deaerated with nitrogen bubbling starting at least 30 min before the experiments.

2.3. *Experiments*

The electrochemical experiments were carried out in a two-compartment cell made of Teflon. The reference electrode compartment was connected to the working electrode compartment with a Luggin capillary of 2 mm in diameter, filled with an asbestos thread soaked in the test solution.

Cyclic voltammetry and potentiodynamic studies were realized with a PAR model 273 potentiostat. All the potentials reported here are referenced to Ag/AgCl,KCl saturated potential; for simplicity, Ag/AgCl label will be used. Potentiodynamic studies were carried out at 0.17 mV s^{-1} from −1300 to 600 mV, whereas cyclic voltammetry studies were done at 50, 100, 200 and 500 mV s^{-1} from −1300 to 0 mV. Three trials were done for each test and the reproducibility of the electrochemical response was improved by starting every test with a 5 min cathodic polarization at −1300 mV. This assured that the reduction of oxides formed spontaneously on the surface before initiating the run. The time and the duration of such polarisation were found to have no influence on the shape of the curves.

Oxide films formed at peak potentials during testing were investigated by scanning electron microscopy (SEM) and X-ray photoelectron spectroscopy (XPS). SEM was performed using a Jeol/Quantek detector combined with Edax analysis whereas XPS analyses were done with a Kratos Axis HS apparatus using a Mg anode at 12 keV.

3. Experimental results

3.1. *Cyclic voltammetry results*

As already mentioned, the general behaviour of 300W carbon steel was determined at 30 and 100 °C in pure NaOH solution. The stable plots obtained (Figures 1 and 2) show the same shape as previously reported [3–8]. The correspondence of peaks was determined by sweeping the potential between different limits (Figure 3).

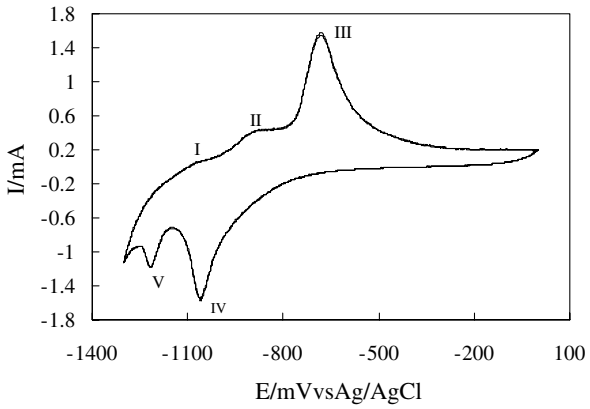

Fig. 1. Stable voltammogram of 300W in 2.25 M NaOH solution at 30 °C, dE/dt = 50 mV s^{-1}.

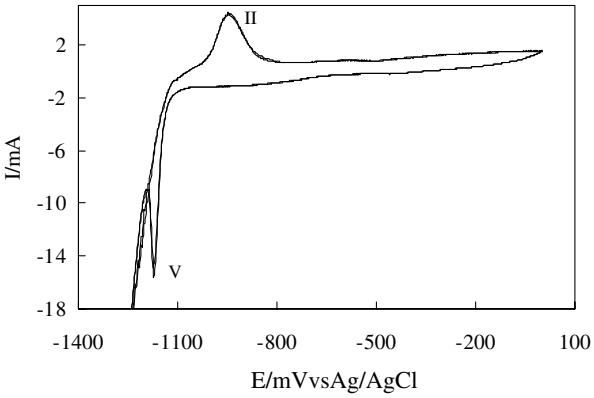

Fig. 2. Stable voltammogram of 300W in 2.25 M NaOH solution at 100 °C, dE/dt = 50 mV s^{-1}.

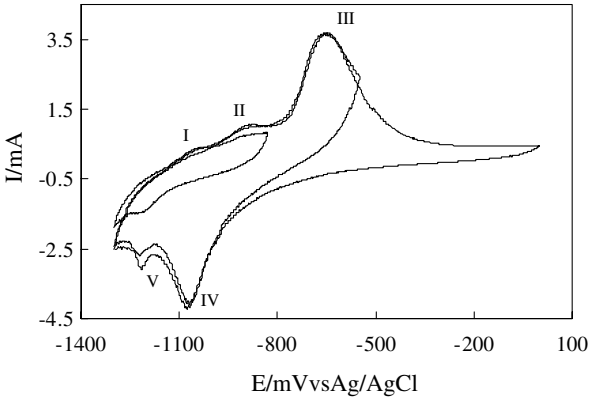

Fig. 3. Effect of different potential limits on cyclic voltammograms in pure NaOH solution at 30 °C, dE/dt = 50 mV s^{-1}.

Thus, peaks I and II are reduced to peak V, whereas peak IV is the conjugate of peak III.

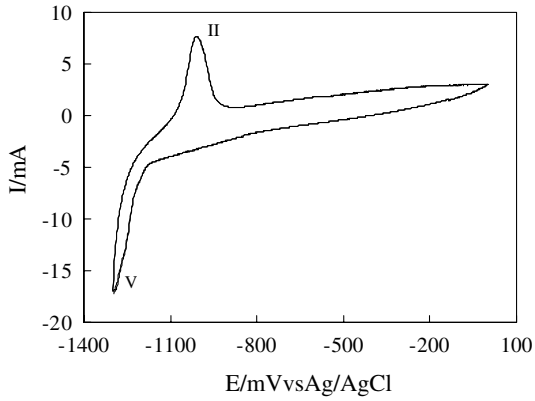

Fig. 4. Stable voltammogram of 300W obtained in a Bayer solution with 75 g l^{-1} of alumina at 100 °C, dE/dt = 50 mV s^{-1}.

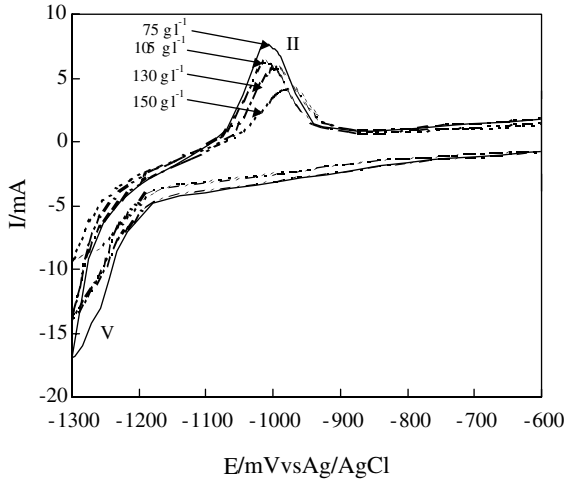

Fig. 5. Influence of alumina content on stable voltammogram, dE/dt = 50 mV s^{-1}. Key: (—) 75, (-·-·) 105, (-···) 130 and (···) 150 g l^{-1}.

A typical cyclic voltammogram obtained at 100 °C in a Bayer solution is presented in Figure 4. The shape of the voltammogram is typical for Bayer solutions [1,3]. Peak II is well defined and is greater than for NaOH solution, meaning that the charge consumed for this process is greater. Peak V, the conjugate of peak II, shifts towards negatively and overlaps the hydrogen evolution reaction. Acquisition of quantitative data for this peak is difficult and its analysis is not presented here.

The influence of alumina concentration on the voltammograms is presented in Figure 5. The anodic part of the curve is not completely presented to allow a better understanding of the evolution of the peaks. The increase in alumina concentration decreases the intensity of peak II and shifts it towards more positive values of potential. The same behaviour is observed for all Bayer solutions with different alumina concentrations and the scan rates used (Figures 6 and 7). Good linearity was found for peak potential E_p and peak current I_p as a function of the square root of the scan rate $v^{1/2}$.

The non-faradaic component of the current can be ignored since its value was found to be 19 μA for the highest sweep rate used. This value was calculated by

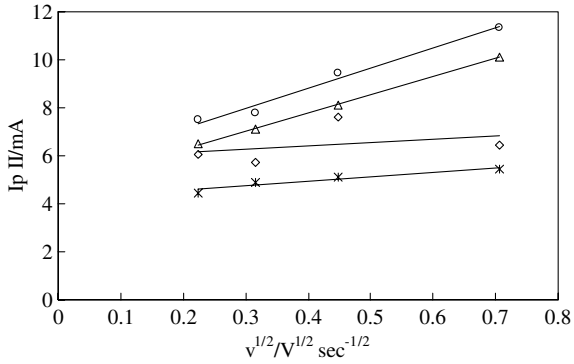

Fig. 6. Variation of peak II current for different alumina concentrations and scan rates. Key: (○) 75, (△) 105, (◇) 130 and (∗) 150 g l^{-1}.

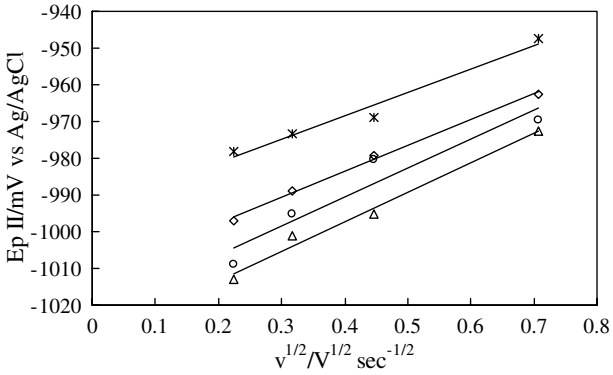

Fig. 7. Variation of peak II potential for different alumina concentrations and scan rates. Key: (○) 75, (△) 105, (◇) 130 and (∗) 150 g l^{-1}.

giving a maximum value of 100 μF cm^{-2} for the double-layer capacity of the metal electrode in aqueous solutions over the entire potential range studied. Thus, the current response principally comes from the charge transfer processes at the metal surface.

The total anodic and cathodic charges decrease with increase in the sweep rate. The dependence of charge on sweep rate indicates that mass transfer control appears either in the solution or within the oxide formed on the surface. Additionally, the charge decreased with increasing alumina concentration (Figure 8). It was also found that the cathodic charge is greater than the anodic charge for almost all sweep rates. This may be the result of overlapping of peak V and the hydrogen evolution reaction.

3.2. *Potentiodynamic results*

The polarisation curves obtained for 300W carbon steel in hot Bayer solutions are presented in Figure 9.

Two current peaks are present on the curves, peaks II and III. Peak II has a well defined shape for all aluminate concentrations whereas peak III becomes larger and less sharp when decreasing aluminate concentration. Increasing aluminate concentration decreases the current density values for anodic peak II and shifts the potential value in the noble direction (Figure 10).

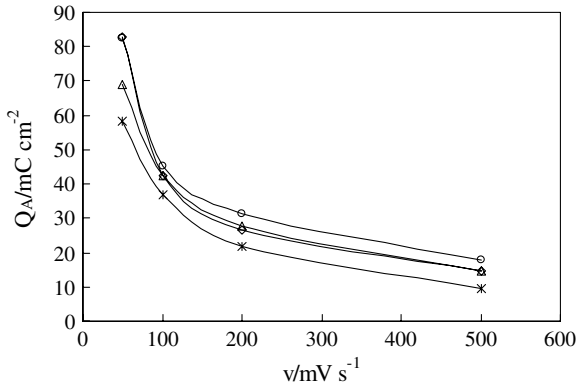

Fig. 8. Variation of total anodic charge with sweep rate and alumina concentrations. Key: (○) 75, (△) 105, (◇) 130 and (∗) 150 g l^{-1}.

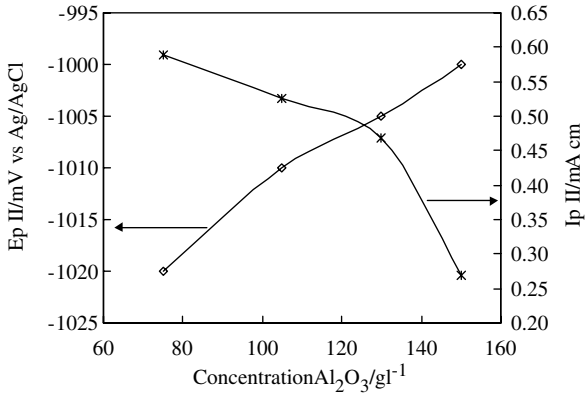

Fig. 10. Influence of alumina concentration on peak II potentials (◇) and currents (∗) .

3.3. *Surface analyses results*

The influence of alumina content on morphology and chemical composition of oxide films formed on the electrode surface was investigated. Oxide films were prepared by scanning the potential at 50 mV s^{-1} between −1300 and −970 mV vs Ag/AgCl, just above peak II. SEM analyses show that the oxide obtained for 75 g l^{-1} alumina concentration presents well defined octahedral crystals, while upon increasing the alumina content, the size of crystals is reduced. Therefore, it became increasingly difficult to determine the crystal structure (Figure 11). The EDX spectra of oxides, for all alumina concentrations, indicate that the Al was present in the film. X-ray diffraction failed to identify the oxide film, compositions probably because the films were too thin. XPS analyses were performed to determine the depth profile concentration of the oxide films. The main elements seen on the surface are Fe, C, O and Al, with some traces of Na, Ti and Cu. The depth profile spectrum is presented in Figure 12. It was found that the aluminium signal was present throughout the oxide layer for all alumina concentrations but was reduced to almost zero into the substrate. No specific correlation can be determined between alumina content in oxide film and alumina concentration in solution. For all the oxides obtained in the Bayer solution with different alumina concentration, the alumina concentration decreases from the oxide surface to the electrode surface.

4. Discussion

Already, much work has been done to identify the peaks obtained by cyclic voltammetry in NaOH solutions. At low temperatures (Figure 1), peak I is associated with hydrogen desorption [9, 10] or $Fe(OH)_2$ formation [5, 8]. At peak II, active dissolution of iron is reported, with formation of $Fe(OH)_2$ and its subsequent transformation into Fe_3O_4. The evolution of anodic peak III is opposite to that of the anodic peaks I and II, suggesting that the reaction at peak III can take place in the same

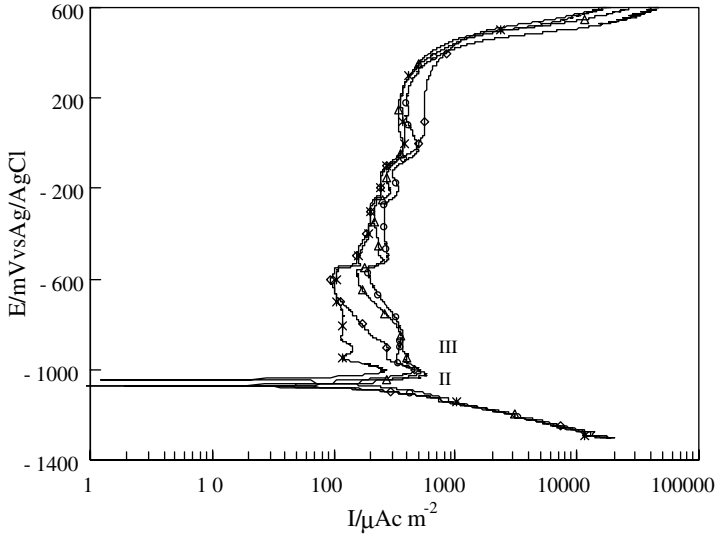

Fig. 9. Polarization curves for 300W carbon steel in Bayer solutions with different aluminate concentrations. Key: (○) 75, (△) 105, (◇) 130 and (∗) 150 g l^{-1}.

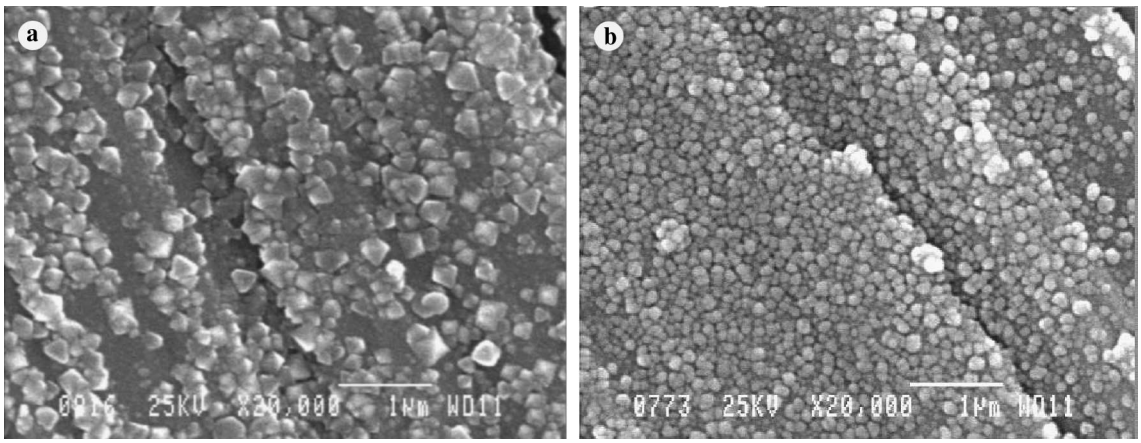

Fig. 11. Oxide films formed for different alumina content: (a) 75 g l^{-1} and (b) 130 g l^{-1}.

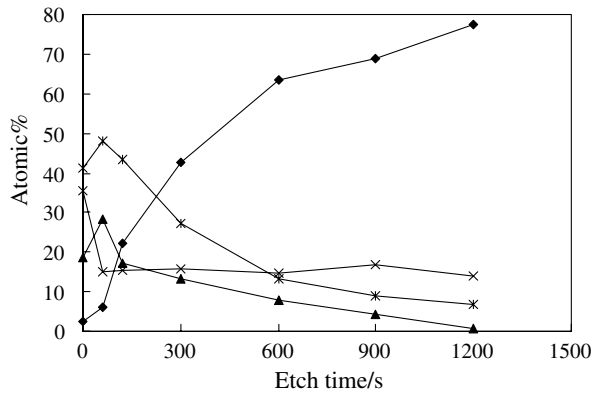

Fig. 12. Depth profiling of oxide film formed in a Bayer liquor with 75 g l^{-1} alumina at 100 °C. Key: (♦) Fe 2p, (∗) O 1s, (×) C 1s and (▲) Al 2p.

time or after those corresponding to peaks I and II [4, 5]. FeOOH formation is obtained at this peak, the process being either parallel or consecutive. Thus, the oxidation of the residual $Fe(OH)_2$, remaining after its transformation to Fe_3O_4, or the direct oxidation of Fe into FeOOH, with $Fe(OH)_2$ as intermediary species, are the possible reactions at this peak. Schrebler et al. [8] took into account the consecutive process only and confirmed the presence of FeOOH at this potential level. Other researchers also confirmed the presence of FeOOH at this level of potential [11–13]. After peak III, the passive film is mainly formed of Fe_2O_3 since it can be stated that the oxidation of magnetite takes place [5, 8, 10, 13].

At high temperatures (Figure 2), iron dissolution is very important [9, 14] and peak II becomes the principal peak on the voltammogram. Fe_3O_4 is directly formed at this peak. For potentials higher than that of peak II, oxidation of Fe_3O_4 to Fe_2O_3 (possibly to FeOOH) is observed. For the reduction peaks, the opposite reactions are obtained at low and high temperatures.

Cyclic voltammograms obtained in Bayer plant solutions at 100 °C (Figure 5) present only one charge transfer process at peak II, between hydrogen and oxygen evolution. It was found that the peak currents for peak II are proportional to the square root of the sweep rate, indicating that mass transport rather than surface adsorption control the charge transfer process (Figure 6). The diffusion of hydroxyl ions to the metal surface is possibly responsible for this. The dependence of peak potential on sweep rate shows that the charge transfer process is irreversible. Moreover, it was observed that the peak potentials shift positively with increasing sweep potential rate and with increasing alumina concentration, meaning that the process at this peak becomes increasingly difficult.

Although a fraction of the oxides formed during anodic polarisation is not reduced (irreversible processes), the total charge for the oxidation process is less than that obtained for the reduction process for most scan rates. This difference can be mainly due to the hydrogen evolution reaction, which is difficult to separate from the reduction peak V. As can be seen in Figure 8, there is a decrease in the total anodic charge when the alumina content increases in Bayer plant solution. This would reveal the inhibiting effect of alumina on iron dissolution. Consequently, the total cathodic charge also decreases.

To identify the oxides formed in Bayer plant solutions at 100 °C, an *E*–pH diagram by Le [15], for the system Fe–H_2O at 100 °C, was used. He considered the more precise thermodynamic values proposed by Baes and Mesmer [16] and Naumov et al. [17] as well as the novel *E*–pH diagram done by Silverman [18]. Silverman showed, for the first time, the $Fe(OH)_2$ region between Fe and Fe_3O_4 regions. Moreover, he replaced $HFeO_2^-$ ion with $Fe(OH)_3^-$ ion, the difference between the two species being one water molecule. Based on these results, the thermodynamic values for different equilibrium reactions, which are most favourable at pH 14, were calculated considering that the activity of ions in solution is 10^{-6} M:

$$\begin{aligned} &Fe(OH)_3^- + 3\,H^+ + 2\,e^- \rightarrow Fe + 3\,H_2O \\ &E = 0.510 - 0.111\,pH + 0.037\log[Fe(OH)_3^-] \\ &\quad = -1266\,mV \text{ vs NHE}(-1463\,mV \text{ vs Ag/AgCl}) \end{aligned} \quad (1)$$

$$Fe_3O_4 + 5\,H_2O + 2\,e^- \rightarrow 3\,Fe(OH)_3^- + H^+$$
$$E = -2.018 + 0.037\,pH - 0.111\log[Fe(OH)_3^-]$$
$$= -834\,mV \text{ vs NHE}(-1031\,mV \text{ vs Ag/AgCl}) \quad (2)$$

$$Fe_3O_4 + 8\,H^+ + 8\,e^- \rightarrow 3\,Fe + 4\,H_2O$$
$$E = -0.122 - 0.074\,pH$$
$$= -1158\,mV \text{ vs NHE}(-1355\,mV \text{ vs Ag/AgCl}) \quad (3)$$

$$Fe(OH)_2 + 2\,H^+ + 2\,e^- \rightarrow Fe + 2\,H_2O$$
$$E = -0.118 - 0.074\,pH$$
$$= -1154\,mV \text{ vs NHE}(-1351\,mV \text{ vs Ag/AgCl}) \quad (4)$$

$$3\,Fe_2O_3 + 2\,H^+ + 2\,e^- \rightarrow 2\,Fe_3O_4 + 2\,H_2O$$
$$E = 0.249 - 0.074\,pH$$
$$= -787\,mV \text{ vs NHE}(-984\,mV \text{ vs Ag/AgCl}) \quad (5)$$

Comparison of these values with those obtained for peak II (between −978 and −1013 mV at 50 mV s^{-1}) in Bayer plant solutions gives information related to the oxidation mechanism. Since the potential of peak II is more anodic than the thermodynamically calculated value for Fe_3O_4, it can be deduced that Equation 2 is the dominant one and the principal product of the peak is the Fe_3O_4. However, the subsequent oxidation of magnetite sometimes coincides with the peak potential. It can be stated that the Fe_3O_4 and Fe_2O_3 are the products formed at this peak. Sriram and Tromans found the same correlation but they considered $HFeO_2^-$ species rather than $Fe(OH)_3^-$ species.

SEM and XPS analyses confirm the presence of aluminium in the oxide formed on the surface. Aluminate ions (AlO_2^-) have been reported to inhibit anodic dissolution of the iron in caustic solutions [1, 2]. This behaviour has been ascribed to its absorption on the metal surface and its incorporation in iron oxide formed. It suggests the formation of a mixed iron oxide–iron aluminate spinel $Fe_{3-x}Al_xO_4$.

In the present study, $Al(OH)_4^-$ ion rather than AlO_2^- is considered. Recent thermodynamic study [19] on gibbsite solubility in Bayer liquors has shown that $Al(OH)_4^-$ provides more valid data at high temperatures.

$$Al(OH)_3 + NaOH \rightarrow Na^+ + Al(OH)_4^- \quad (6)$$

The oxide film is supposed to be the same as reported in [1] and [2], but the suggested reaction leading to this compound is different:

$$x\,FeAl(OH)_{4\,ads}^- + (3-x)Fe(OH)_3^- + (1+x)H^+ \rightarrow Fe_{3-x}Al_xO_4 + (x+5)H_2O + x\,Fe + (x+1)e^- \quad (7)$$

Figure 10 shows that peak II is shifted in the positive direction with the increase in alumina concentration. This fact indicates that the kinetics of passivation necessitate higher potentials with the increase in alumina concentration. Further, the current of passivation (peak II) decreases with alumina concentration, indicating the facility of passive film formation. Finally, it can be speculated that increase in alumina concentration facilitates the passivation, even if the potential is shifted into the noble direction. The same observation can also be deduced from cyclic voltammetry results (Figures 6 and 7).

Usually, the passivation current reflects the degree of oxide-free surface. Figure 9 shows that the passivation currents diminished with increase in alumina concentration. From the SEM analysis presented in Figure 11, it can be observed that the coverage of the surface by the oxides increased with alumina concentration since the crystals became increasingly finer leading to a less porous film. These observations, related to the linear relationship of I_p and E_p vs $v^{1/2}$ found in cyclic voltammetry, indicate that the pore resistance model [4, 20, 21] can be extrapolated here. The model assumes that a passive film of constant thickness is formed and spread laterally on the surface until a small fraction of the surface rests uncovered. The dissolution is therefore limited at these pores and it seems that diffusion through these pores would be the rate-determining process. At this point, a current drop is observed due to the increase in surface coverage. It can then be stated that alumina behaves as an anodic inhibitor in Bayer plant solutions, not only for passivation but also for the quality of the passive layer.

5. Conclusions

Voltammetry shows that increase in alumina concentration does not change the mechanism of oxidation of iron in Bayer solution. Increasing alumina concentration reduces the critical current of passivation and shifts the critical passivation potential towards noble values. This behaviour is characteristic of anodic inhibitors. The oxide film formed seems to obey the film formation behaviour described in the pore resistance model. Increase in alumina concentration leads to a better coverage of the surface and generates a less porous film formed constituted by fine crystals. Aluminium is found in the oxide films formed and the formation of an oxide containing alumina and iron species is confirmed.

Acknowledgements

The authors would like to acknowledge support from Alcan International Limited and Alcan Vaudreuil Plant. The authors are indebted to Hélène Dufour from the

Analytical Group of the Arvida Research and Development Centre for SEM analyses as well as Emily Smith from the Analytical Group of the Banbury Research and Development Centre for XPS analyses. The support for experimental work provided by Pierre Fournier is greatly acknowledged.

References

1. R. Sriram and D. Tromans, *Corros. Sci.* **25** (1985) 79.
2. S.-E. Liu, Z. Zhu and K. Wei, *Scripta Metallurgica et Materialia* **31** (1994) 427.
3. H.H. Le and E. Ghali, *Corros. Sci.* **30** (1990) 117.
4. D.D. Macdonald and B. Roberts, *Electrochim. Acta* **23** (1978) 781.
5. D.D. Macdonald and D. Owen, *J. Electrochem. Soc.* **120** (1973) 317.
6. A. Wieckowski, E. Ghali and H.H. Le, *J. Electrochem. Soc.* **131** (1984) 2024.
7. A. Wieckowski and E. Ghali, *Electrochim. Acta* **30** (1985) 1423.
8. R.S. Schrebler Guzman, J.R. Vilche and A.J. Arvia, *Electrochim. Acta* **24** (1979) 395.
9. R.D. Armstrong and I. Baurhoo, *J. Electroanal. Chem.* **40** (1972) 325.
10. D. Geana, A.A. El Miligy and W.J. Lorenz, *J. Appl. Electrochem.* **4** (1974) 337.
11. T. Zackroczmski, F. Chwei-Jer and Z. Szklarska-Smialowska, *J. Electrochem. Soc.* **132** (1985) 2862.
12. B. Kabanov, R. Burstein and A. Frumkin, *Discuss. Faraday Soc.* **111** (1947) 493.
13. L. Ojefors, *J. Electrochem. Soc.* **123** (1976) 1691.
14. R.D. Armstrong and I. Baurhoo, *J. Electroanal. Chem.* **34** (1972) 41.
15. H.H. Le, Thèse de doctorat, (Université Laval, Québec, 1990) p. 254.
16. C.F. Baes and R.E. Mesmer, 'The Hydrolysis of Cations' (J. Wiley & Sons, New York, 1976).
17. G.B. Naumov, B.N. Ryzhenko and I.L. Khodavsky, 'Handbook of Thermodynamic Data' (1974).
18. D.C. Silverman, *Corrosion* **10** (1982) 343.
19. S.P. Rosenberg and S.J. Healy, *in* Fourth International Alumina Quality Workshop, Darwin (1996).
20. W.J. Müller, *Trans. Faraday Soc.* **27** (1931) 737.
21. A.J. Calandra, N.R. Tacconi, R. Pereiro and A.J. Arvia, *Electrochim. Acta* **19** (1974) 901.